ELSEVIER

Journal of Power Sources 86 (2000) 363–368

JOURNAL OF POWER SOURCES

www.elsevier.com/locate/jpowsour

Optimisation of flow-field in polymer electrolyte membrane fuel cells using computational fluid dynamics techniques

E. Hontañón [a,*], M.J. Escudero [a], C. Bautista [a], P.L. García-Ybarra [a], L. Daza [a,b]

[a] *Fossil Fuel Department, CIEMAT, Avda. Complutense 22, 28040 Madrid, Spain*
[b] *Instituto de Catálisis y Petroleoquímica, CSIC, Campus UAM-Cantoblanco, 28049 Madrid, Spain*

Accepted 12 November 1999

Abstract

The purpose of this work was the enhancement of performance of Polymer Electrolyte Membrane Fuel Cells (PEMFC) by optimising the gas flow distribution system. To achieve this, 3D numerical simulations of the gas flow in the assembly, consisting of the fuel side of the bipolar plate and the anode, were performed using a commercial Computational Fluid Dynamics (CFD) software, the ''FLUENT'' package. Two types of flow distributors were investigated: a grooved plate with parallel channels of the type commonly used in commercial fuel cells, and a porous material. The simulation showed that the permeability of the gas flow distributor is a key parameter affecting the consumption of reactant gas in the electrodes. Fuel utilisation increased when decreasing the permeability of the flow distributor. In particular, fuel consumption increased significantly when the permeability of the porous material decreased to values below that of the anode. This effect was not observed in the grooved plate, which permeability was higher than that of the anode. Even though the permeability of the grooved plate can be diminished by reducing the width of the channels, values lower than 1 mm are difficult to attain in practice. The simulation shows that porous materials are more advantageous than grooved plates in terms of reactant gas utilisation.

Keywords: Polymer electrolyte membrane fuel cells; Gas flow distribution; Computational fluid dynamics; Grooved plate; Porous materials

1. Introduction

Most experimental investigations of fuel cells are expensive. In addition, they can only be carried out on a small scale, with a few designs and with difficulties of measurement. On the other hand, the cost of numerical modelling of fuel cells is low, and it is easy to set up a number of alternative designs. Here, 3D numerical simulation of gas transport and distribution in the anode of a PEMFC in contact with a gas flow distributor has been performed using a commercial CFD computer code, the FLUENT package [1]. The objective was to optimise the design of the gas flow distribution system for PEMFCs. The flow distributor commonly used in commercial fuel cells consists of a grooved plate with parallel ribs and channels. Numerical simulations were performed in order to identify the optimal width and number of channels in the grooved plate, for which the fuel consumption in the anode is the highest. In addition, simulations were also performed for a porous material acting as gas distributor, with permeability varying over a wide range of values. The performance of the two flow distributors was assessed in terms of fuel utilisation in the anode, and compared to each other. The results of the simulation show that fuel consumption increases when decreasing the permeability of the gas distributor. The reason is that by increasing the flow resistance of the medium over the front surface of the electrode, the gas is forced to flow deeper into the matrix of the electrode instead of flowing over its surface. In this way, transport of the reactant gas is converted from a diffusion mechanism to a forced convection mechanism. The simulation indicates that in terms of reactant gas utilisation, porous materials are more advantageous than grooved plates. In the first place, the permeability of the grooved plate decreases when decreasing the width and the number of channels. However, channels narrower than 1 mm are not viable in practice, which limits the lowest permeability attainable in flow distributors of this type. Secondly, the ribs of the grooved plate represent a disad-

* Corresponding author. Tel.: +34-91-346-6734; fax: +34-91-346-6269; e-mail: esther@ibm1.ciemat.es

0378-7753/00/$ - see front matter
PII: S0378-7753(99)00478-4

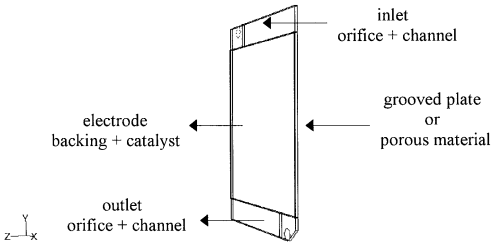

Fig. 1. Configuration assumed in the simulation with FLUENT of a PEMFC.

vantage in comparison with the porous material, since the regions of the electrode surface hindered by the ribs are not effective for gas flow into the electrode.

2. Flow distributor

As attention focused on the gas flow distributor, no attempt was made to model the whole fuel cell. The assembly depicted in Fig. 1, which consists of the fuel side of the bipolar plate and the anode, was considered. The dimensions of the various regions, which were imposed by the bipolar plate and the membrane–electrode assembly, MEA, chosen for this work, are summarised in Table 1. A series of preliminary calculations was performed in order to determine the optimum mesh for the simulation, taking into account the computational time and dynamic memory restrictions imposed by the computer in which FLUENT was run (HP 9000/782). Then, it was decided to use grid dimensions listed in Table 2. The catalyst layer consisted of a single node of width equal to the grid spacing in the *z*-direction (60 μm). Typically, the thickness of the catalyst zone varies between 5 and 15 μm, compared to the value assumed in the simulation, 60 μm, which is relatively large. For the dimensions given in Table 1, a computational mesh of about 235 000 volume elements was obtained with the grid shown in Table 2.

3. Flow dynamics model

Numerical simulations were performed with FLUENT version 5.1.1. It was assumed that the fuel was hydrogen, and the flow regime was laminar. Stationary and isothermal conditions were also assured within the fuel cell, too. Then, the conservation laws of mass and momentum, which govern fluid dynamics in the inlet and outlet channels of the gas distributor are:

$$\nabla(\rho\vec{v}) = 0 \tag{1}$$

$$\vec{\nabla}(\rho\vec{v}\vec{v} - \tau + P) = 0 \tag{2}$$

where τ is the stress tensor. On the other hand, the pressure drop in a fluid passing through a homogeneous porous medium is taken into account in FLUENT by means of the expression:

$$\vec{\nabla}P = \frac{\mu}{\alpha}\vec{v} + \frac{1}{2}\mathrm{C}\rho|\vec{v}|\vec{v} \tag{3}$$

where the first and second terms on the right-hand side represent the viscous and the inertial losses, respectively. Viscous losses, given by Darcy's law, are proportional to the flow velocity; the resistance coefficient depends on the permeability of the medium, α. Inertial losses are proportional to the square of the flow velocity. At low flow velocities, like those expected in fuel cells, the pressure drop will be dominated by the viscous term and inertia can be neglected. Thus, the momentum equation for porous media takes the form:

$$\vec{\nabla}(\rho\vec{v}\vec{v} - \tau + P) - \frac{\mu}{\alpha}\vec{v} = 0 \tag{4}$$

which is accurate up to $O(v^2)$ inside the porous medium, but ensures a continuous matching to the free flow solution, when $\alpha \to \infty$ and $C \to 0$.

4. Gas reaction model

It was assumed that hydrogen oxidation at the anode could be described by two-step kinetics of the Michaelis–Menten type [2]

$$\mathrm{H_2} + \mathrm{Pt} \underset{k_{-1}}{\overset{k_1}{\leftrightarrow}} c^* \overset{k_2}{\rightarrow} 2\mathrm{H^+} + 2\mathrm{e^-}$$

where $\mathrm{H_2}$ is the reactant, Pt is the catalyst, c^* is a reactant–catalyst complex, and $\mathrm{H^+}$ is the final product of

Table 1
Dimensions of the PEMFC components

Direction	(mm)	Inlet/outlet[a] channels	Grooved plate/porous material	Electrode	
				Backing	Catalyst
x	length *L*	70	70	70	70
y	height *H*	10	70	70	70
z	width Δ*z*	1	1	0.24	0.06

[a]The diameter of the gas inlet/outlet orifice was 5 mm.

Table 2
Computational grid used in the simulation with FLUENT of the PEMFC

(mm)	Inlet/outlet channels	Grooved plate/porous material	Electrode		Number of nodes
			Backing	Catalyst	
Δx	0.5	0.5	0.5	0.5	140
Δy	0.5	0.5	0.5	0.5	180
Δz	0.2	0.2	0.06	0.06	10

the reaction. The velocity constants of the reactions involved, k_i, have the following meaning: k_1 stands for the rate of molecular hydrogen adsorption and dissociation onto the platinum particles, k_{-1} controls the rate of the inverse atomic hydrogen recombination and desorption processes, and k_2 governs the rate of atomic hydrogen oxidation. The rest of the fuel cell components, which were not considered in this work, influence the oxidation of atomic hydrogen at the catalyst sites. Thus, k_2 is a function of the parameters, which determines the state of the fuel cell. By assuming that the initial concentration of H_2 is much larger than that of Pt, it is found that the hydrogen depletion rate obeys a law of the type:

$$\frac{d\rho}{dt} = -\frac{\lambda\rho}{\rho+\kappa} \tag{5}$$

where ρ is the concentration of hydrogen, and the coefficients λ and κ have the form:

$$\lambda = k_2 \frac{M_{H_2}}{M_{Pt}} \rho^{o}_{Pt} \tag{6}$$

$$\kappa = \frac{k_{-1}+k_2}{k_1 \dfrac{N_A}{M_{Pt}}} \tag{7}$$

with ρ^{o}_{Pt} being the initial concentration of platinum in the catalyst layer; M_{H_2} and M_{Pt} the molecular weight of hydrogen and platinum, respectively, and N_A, Avogadro's number. Therefore, in the catalyst layer, the mass and momentum conservation equations take the form:

$$\nabla(\rho\vec{v}) = S_\rho \tag{8}$$

$$\vec{\nabla}(\rho\vec{v}\vec{v} - \tau + P) - \frac{\mu}{\alpha}\vec{v} = \vec{S}_m \tag{9}$$

where S_ρ and S_m represent the sink terms of mass and momentum, which are evaluated by means of the formulae:

$$S_\rho = -\frac{\lambda\rho}{\rho+\kappa} \tag{10}$$

$$\vec{S}_m = S_\rho\vec{v} \tag{11}$$

The coefficients λ and κ depend on the velocity reaction constants and the initial concentration of platinum in the catalyst layer. In a fuel cell, atomic hydrogen recombination and desorption are expected to be minor processes, $k_{-1} \ll k_2$, so that

$$\lambda = k_2 \frac{M_{H_2}}{M_{Pt}} \rho^{o}_{Pt} \tag{12}$$

$$\kappa = \frac{k_2 M_{Pt}}{k_1 N_A} \tag{13}$$

given the lack of data on the velocity constants k_1 and k_2, we decided to set κ at unity ($\kappa = 1$) and let λ vary proportionally with ρ^{o}_{Pt}. Thus, different values of λ are associated with different values of the concentration of platinum initially in the catalyst layer. It may be noted that Eq. (5) was derived for reactions in the gaseous phase, where the volumetric reaction rate is given by $-k_1 n n_{Pt}$; with n and n_{Pt} being the molecular concentration (mol cm^{-3}) of H_2 and Pt, respectively, and k_1 the collision frequency ($cm^3\ s^{-1}$). In terms of mass concentration, the volumetric reaction rate has the form $-k_1(M_{H_2}M_{Pt}/N_A^2)\rho\rho_{Pt}$. In the anode, the rate of hydrogen adsorption on the surface of the platinum particles is expressed as $-k_1(M_{H_2}M_{Pt}/N_A^2)\rho m_{Pt}/\delta$; where m_{Pt} is the platinum loading per unit geometric area of the anode ($mg_{Pt}\ cm^{-2}$), and δ is the thickness of the catalyst layer.

5. Results and discussion

Two sets of parametric calculations were performed corresponding to the grooved plate and the porous material. The following boundary conditions were imposed in all the cases: temperature = 60°C, outlet pressure = 1 bar, and gas inlet velocity = 0.3 m s^{-1} (0.4 lN min^{-1}). It was assumed that the anode was a fibrous graphite cloth with a porosity of 74% and a mean fibre diameter of 15 μm (National Electric Carbon). Then, the permeability of the anode was estimated from the database on fibrous materials available in Ref. [3], and the resulting value was 5.5×10^{-11} m^2. Finally, values of λ were chosen equal to 1, 5, and 10, which led to hydrogen consumption fractions of about 5%, 25%, and 45% (weight), respectively.

5.1. Grooved plate

There were two free parameters in the simulation of the grooved plate, which are the width of the solid ribs, Δx_r,

and the width of the flow channels, Δx_c. As a reference, a base case we considered (run 0) corresponding to the commercial bipolar plate of graphite (Electrochem) presently used in our laboratory ($\Delta x_r = 1$ mm, $\Delta x_c = 2$ mm) [4]. Then, three series of calculations were performed, the results of which are shown in Table 3. In series 1, the width of the ribs were kept constant ($\Delta x_r = 1$ mm) and the width of the channels varied ($\Delta x_c = 2$, 1, 0.5 mm). By reducing the width of the channels, the number of flow tracks increased. As can be seen in Table 3, the H_2 consumption in the anode rose when reducing the width of the channels. In series 2, the width of the channels were constant ($\Delta x_c = 1$ mm) and the width of the ribs varied ($\Delta x_r = 1$, 2, 3, 4 mm). When increasing the width of the ribs, the number of flow tracks diminished. Table 3 shows that H_2 depletion in the anode increased with the rib width. In series 3, ribs and channels were assumed to be of the same size and Δx_r and Δx_c were varied together ($\Delta x_r = \Delta x_c = 0.5$, 1, 2 mm). As shown in Table 3, the consumption of H_2 in the anode rose when the size of ribs and channels decreased.

The predictions of simulation are consistent with the experimental results obtained by Hentall et al. [5]. These authors investigated the contribution that the tracks of the current collecting plates make to the overall performance of a PEMFC similar to the one studied here (70×70 mm^2). To do that, they carried out a series of experiments in which the width of channels and ribs was varied while keeping all other parameters constant. The performance of the cells with $\Delta x_r = 1$ mm increased when the width of the channels was reduced ($\Delta x_c = 4$, 2, 1 mm), while the performance of the cells with $\Delta x_c = 1$ mm showed a smaller effect when the width of the ribs was increased ($\Delta x_r = 1$, 2, 4 mm). Besides, Hentall et al. performed several tests with $\Delta x_r = \Delta x_c = 4$, 2, 1 mm; they observed that decreasing the size of both ribs and channels was clearly advantageous for the fuel cell performance.

5.2. Porous material

Regarding the porous material, which plays the role of gas distributor, a fibrous material has been considered here. For each value of λ, a total of nine calculations we performed, covering a wide range of permeability values, from 5.5×10^{-12} to 5.5×10^{-8} m^2. The values of the mass fraction of H_2 consumed in the anode calculated with FLUENT are summarised in Table 4. The maximum consumption of H_2 corresponds with the lowest permeability value, $\alpha = 5.5 \times 10^{-12}$ m^2. This is the only calculation in which the permeability of the porous material was inferior to the permeability of the anode, $\alpha = 5.5 \times 10^{-11}$ m^2. The consumption of H_2 shows a plateau in the region of permeability values close, or higher than that of the anode, and decreases abruptly for values of α above 10^{-8} m^2. Thus, the results reveal that highly permeable materials are not advantageous for gas flow distribution in fuel cells, hence, the use of porous materials less permeable than the electrodes must be recommended.

Table 3
H_2 consumption in the anode in the simulation of the grooved plate

Run	Dimensions		H_2 consumption mass fraction (%)		
	Δx_r (mm)	Δx_c (mm)	$\lambda = 1$	$\lambda = 5$	$\lambda = 10$
0	1	2	3.2	21.7	43.7
1	1	1	3.8	21.8	45.4
2	1	0.5	5.1	23.7	47.0
1	1	1	3.8	21.8	45.4
3	2	1	3.9	22.3	45.4
4	3	1	4.0	22.6	45.7
5	4	1	4.1	22.7	45.7
6	2	2	3.5	21.5	44.9
1	1	1	3.8	21.8	45.4
7	0.5	0.5	3.9	22.8	46.4

Table 4
H_2 consumption in the anode in the simulation of the porous material

α (m^2)	H_2 consumption mass fraction (%)		
	$\lambda = 1$	$\lambda = 5$	$\lambda = 10$
5.5×10^{-12}	6.0	25.4	49.2
5.5×10^{-11}	5.2	23.4	47.2
5.5×10^{-10}	5.5	24.4	47.4
1.1×10^{-9}	5.8	24.3	47.5
5.5×10^{-9}	5.6	24.5	47.6
1.1×10^{-8}	5.7	24.3	47.6
2.2×10^{-8}	4.6	23.4	46.9
4.4×10^{-8}	3.1	21.9	45.7
5.5×10^{-8}	2.8	21.8	45.6

5.3. Grooved plate vs. porous material

To compare the performance of the two gas flow distributors, the concept of equivalent permeability has been introduced, which is defined as the permeability of the porous medium which causes the same pressure drop as the grooved plate. The pressure drop in a duct follows the Hagen–Poiseuille law [6]

$$\left.\frac{\Delta P}{H}\right|_{\text{channel}} = K\bar{u}_c \tag{14}$$

where H is the height of the duct; K is a coefficient, which depends on the geometry of the conduit and the gas properties; and $\bar{u}_c$ is the average flow velocity in the duct. On the other hand, the pressure drop in a porous medium obeys Darcy's law

$$\left.\frac{\Delta P}{H}\right|_{\substack{\text{porous}\\ \text{medium}}} = \frac{\mu}{\alpha}\bar{u} \tag{15}$$

where $\bar{u}$ is the average flow velocity in the porous material. As the mass flow rate through the grooved plate and the porous medium is the same, the following relationship between $\bar{u}$ and $\bar{u}_c$ exists

$$\bar{u} = \frac{N_c \bar{u}_c \Delta x_c}{L} \tag{16}$$

with N_c being the number of channels, Δx_c the width of the channels, and L the length of either the grooved plate or the porous material. After substituting Eq. (16) and equating Eqs. (14) and (15), the following expression for α is obtained:

$$\alpha = \frac{\mu N_c \Delta x_c}{LK} \tag{17}$$

the expression for K for a rectangular channel of dimensions Δx_c and Δz was found to be:

$$K = \frac{\mu}{(\Delta z/2)^2}\left[\frac{1}{3} - \left(\frac{64}{\pi^5}\right)\frac{\Delta z}{\Delta x_c}\sum_{\substack{n\\ \text{odd}}}^{\infty}\frac{1}{n^5}\tanh\left(\frac{n\pi\Delta x}{2\Delta z}\right)\right]^{-1} \tag{18}$$

so, finally, the equivalent permeability takes the form:

$$\alpha = \frac{N_c(\Delta z/2)^2\Delta x_c}{L} \times\left[\frac{1}{3} - \left(\frac{64}{\pi^5}\right)\frac{\Delta z}{\Delta x_c}\sum_{\substack{n\\ \text{odd}}}^{\infty}\frac{1}{n^5}\tanh\left(\frac{n\pi\Delta x}{2\Delta z}\right)\right] \tag{19}$$

which is a function of geometrical factors only. As shown in Table 1, the dimensions of the grooved plate are $L = 70$ mm and $\Delta z = 1$ mm. Therefore, α depends on two parameters, which are N_c and Δx_c. The values of the equivalent permeability calculated with Eq. (19) for the various configurations of the grooved plate are listed in Table 5. The permeability increases with both the width and the number of channels of the grooved plate.

Fuel consumption is plotted as a function of permeability in Fig. 2, for $\lambda = 5$. Similar trends were observed for $\lambda = 1$, 10. In general, the consumption of hydrogen in the anode increases when decreasing the permeability, particularly when the permeability of the gas flow distributor is lower than that of the anode. Besides, for a given permeability value, hydrogen depletion is lower for a grooved plate than for a porous material. A possible explanation is the presence of the solid ribs in the grooved plate, which causes a reduction of the effective surface area for the gas to flow into the electrode. It is observed that in the simulation, the permeability of the grooved plate ranged from 5×10^{-9} to 4×10^{-8} m^2, which is well above the permeability of the anode, 5.5×10^{-11} m^2. In theory, reducing the width of the channels could attain lower permeability values. However, channels narrower than 0.5 mm are not realisable in practice, so no attempt to simulate them was made.

Table 5
Equivalent permeability of various grooved plate configurations

Run	Channel width Δx_c (mm)	Number of channels N_c	α (m^2)
2	0.5	47	4.8×10^{-9}
7	0.5	70	7.1×10^{-9}
5	1	14	7.0×10^{-9}
4	1	18	9.0×10^{-9}
3	1	24	1.2×10^{-8}
1	1	35	1.8×10^{-8}
6	2	18	2.9×10^{-8}
0	2	24	3.9×10^{-8}

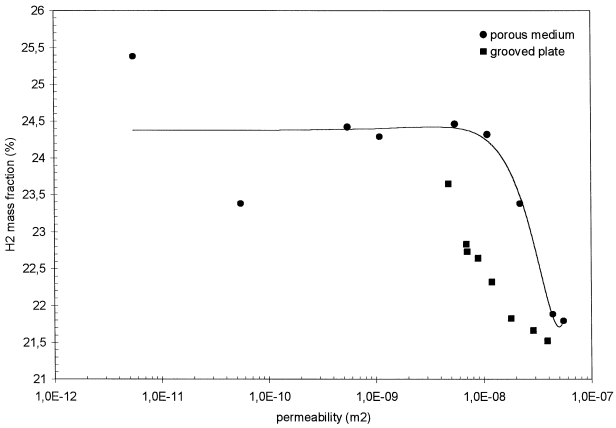

Fig. 2. H_2 consumption in the anode vs. permeability for $\lambda = 5$.

Pressure drop is displayed vs. permeability in Fig. 3, for $\lambda = 5$. As expected, the pressure drop is a decreasing function of the permeability of the medium. The highest pressure drop, corresponding with the material of lowest permeability, was 2.0 kPa. As can be deduced from Figs. 2 and 3, the fuel utilisation in the anode correlates with the pressure drop. The results of the simulation show that by increasing the flow resistance of the gas distributor on the front of the electrode, the gas is forced to flow into the electrode. That way, a larger amount of gas reaches the catalyst region, and gas consumption increases. This behaviour is consistent with that observed in interdigitated gas flow distributors, as shown by Yi and Nguyen [7]. In interdigitated flow distributors, the pressure drop across the ribs forces the reactant gases to flow into the electrodes as compared to flowing over the surface of the electrodes, which is the case in conventional parallel-channel gas distributors, like those treated here. That way, the transport

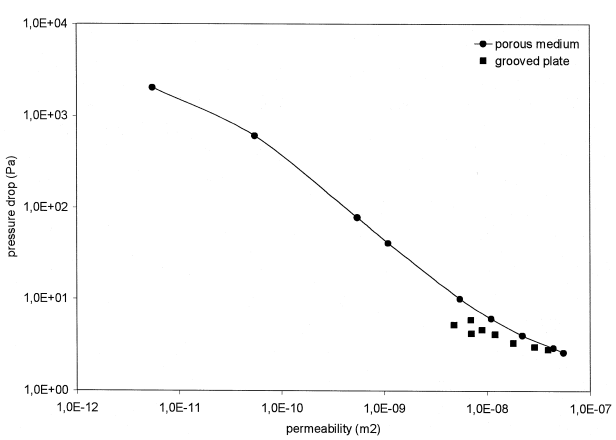

Fig. 3. Pressure drop vs. permeability for $\lambda = 5$.

of the reactant gases is converted from a diffusion mechanism to a forced convection mechanism.

6. Conclusions

3D numerical simulation of the gas flow distribution in a PEMFC has been performed using the FLUENT code. For a bipolar plate and an MEA of specific dimensions (70×70 mm^2), two types of flow distributors have been considered: a grooved plate, and a porous material. The performance of the flow distribution system was assessed in terms of the fuel consumption in the anode. Gas consumption increases when decreasing the permeability of the gas distributor placed on the front of the electrode. The simulation shows that in terms of reactant gas utilisation, porous materials are more advantageous than grooved plates. Therefore, porous materials seem to be promising candidates to be used as gas flow distributors in PEMFCs, and further effort will be devoted to investigate them.

References

[1] FLUENT 5 User's Guide, Fluent, Lebanon, UK, 1998.
[2] C.C. Lin, L.A. Segel, Mathematics applied to deterministic problems in natural sciences, Classics in Applied Mathematics, Vol. I, SIAM, Philadelphia, 1988.
[3] G.W. Jackson, D.F. James, Can. J. Chem. Eng. 64 (1986) 364.
[4] L. Daza, Development of low temperature fuel cells with methanol as a fuel option. Contract JOE3-CT97-0049. Mid-term progress report to the European Commission, 1999.
[5] P.L. Hentall, J.B. Lakeman, G.O. Mepsted, P.L. Adcock, J.M. Moore, J. Power Sources 80 (1999) 235.
[6] G.K. Batchelor, Introducción a la dinámica de fluidos, Ministerio de Medio Ambiente, Dirección General del Instituto Nacional de Meteorología, Madrid, 1997.
[7] J.S. Yi, T.V. Nguyen, J. Electrochem. Soc. 146 (1999) 38.